Simulation of Rock Cutting Behavior of a Single PDC Cutter for Medium-Hard to Hard Formations

Nana Shoji and Shigemi Naganawa

School of International Resource Sciences, Akita University, Japan

Keywords

Geothermal, drilling, PDC bits, uniaxial compression simulation, DEM cutting simulation

ABSTRACT

In oil and gas well drilling, PDC (polycrystalline diamond compact) bits enable a high rate of penetration and a long bit life and are now the most popular drill bit regardless of its high cost. Although PDC bits have the advantage in heat resistant performance compared to roller cone bits, PDC bits generally perform poorly when drilling hard, abrasive, and inhomogeneous volcanic formations encountered in typical geothermal fields. In this study, we conducted numerical simulations to optimize the bit design and operating conditions of PDC bits for drilling medium-hard to hard formation rocks. We used a distinct-element method (DEM) simulator, PFC2D (2-Dimensional Particle Flow Code) developed by the Itasca Consulting Group Inc., to simulate 2-dimensional cutting behavior of a single PDC cutter. In the PFC modeling, a cutter that is defined as a set of walls moves horizontally across a synthetic rock at a specified velocity and a fixed depth of cut. The synthetic rock specimen that consists of bonded particles is rectangular and confined by three frictionless walls on the bottom, left and right sides. Mud column pressure at the bottom hole is applied to the top surface of the rock specimen. Simulations were conducted with various cutter rake angles, cutter velocities and depths of cut for models of Carthage limestone (a medium-hard rock), and Kurahashijima granite (a hard rock). The forces acting on the cutter and damage in the rock were monitored. Three conclusions were obtained from the simulations. Firstly, the DEM simulation provides a rough idea of the cuttings and the fracturing within the medium-hard to hard rocks caused by the cutting action of a single cutter. Secondly, the results indicate that the mean stress on the specimen is small in medium-hard rocks and large in hard rocks when the back-rake angle is set to 15° and the digging rate is increased. Third, the results of the average stress on the cutters also allowed for a rough comparison of the volume of broken cuttings. From these conclusions, we infer that simulation using the DEM is effective in situations where experimentation is difficult.

1. Introduction

In recent years, PDC bits have attracted attention as drilling tools for geothermal wells, but their practical application requires the development of various technologies. One of these is the development of PDC bits that can withstand the hard, abrasive, and heterogeneous volcanic rock layers encountered in typical geothermal fields. Figure 1 shows a schematic diagram of a geothermal power generation system. The purpose of this paper is to evaluate a numerical simulation study conducted to optimize the design and operating conditions of a PDC bit for drilling through medium-hard to hard formations, using the 2D particle flow code PFC2D (Potyondy and Cundall, 2004). The results confirm the validity of the simulations and suggest that they are effective in situations where experiments are difficult. This study is a basic study of simulation and does not compare the results with experiments. Therefore, the validity of the simulation was confirmed by comparison with existing knowledge. Also, the study did not take into account the loss of PDC cutters, wear, or mud circulation.

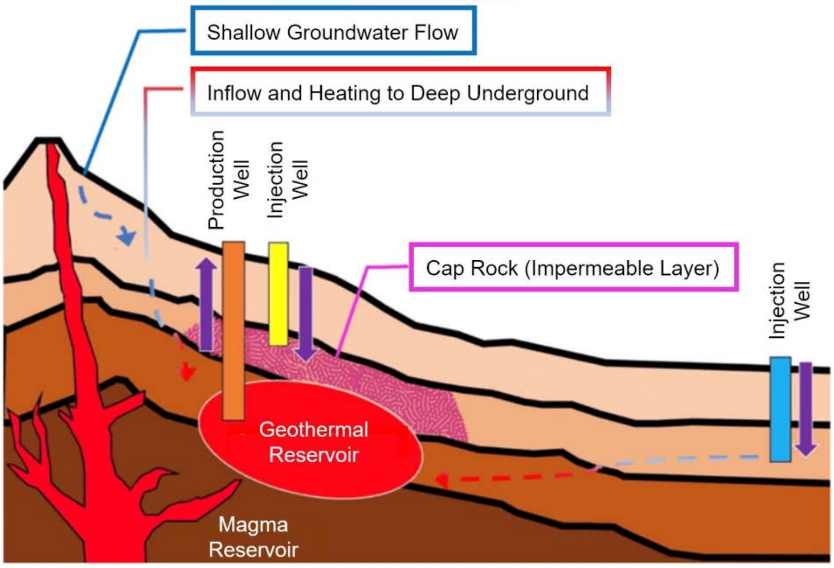

Figure 1: Schematic diagram a geothermal system.

2. Outline of the Simulation

2.1 Experimental Materials and Specimen Preparation

Two types of samples were prepared for the simulations. The simulation of rock creation was based on (Emam and Potyondy, 2010). The physical properties of limestone were taken from (Emam and Potyondy, 2010), and those of granite from (Kaneko et al., 1987). Carthage limestone from the Republic of Tunisia was used as the medium-hard rock, and Kurahashijima granite from Japan was used as the hard rock. The physical properties of each rock were input into PFC2D to create two specimen models.

In Table 1, ρ and ρ_b are the bulk rock density and particle density, respectively; n is the porosity; d is the particle diameter; E_c is the young's modulus at each particle-particle contact; k_n/k_s is the ratio of particle-particle bond normal to shear stiffness; μ is the particle friction coefficient; $\bar{\sigma}_c$ and $\bar{\tau}_c$ are the normal and shear strength, respectively, of the cement-like material represented by a parallel bond. Note that the three micro-parameters for particle-particle contact ($E_{c,}$ k_n/k_s μ) must also be specified, in addition to the fine parallel-bond micro-parameters to characterize a parallel-bonded materials. The normal stiffness is set based on the elastic modulus and particle diameter using the relationship of Potyondy and Cundall (2004).

Table 1: Input data for the PFC2D short-term micro-properties for specimen.

Carthage Limestone		Kurahashijima Granite	
Grain (particle)	Cement (parallel bond)	Grain (particle)	Cement (parallel bond)
ρ= 2620 kg/m^3 (bulk rock density) $\rho_b = \frac{\rho}{1-n}$ = 3196 kg/m^3 (n=0.17)		ρ= 2630 kg/m^3 (bulk rock density) $\rho_b = \frac{\rho}{1-n}$ = 3169 kg/m^3 (n=0.17)	
(d_{max}/d_{min}) = 1.66, d_{min} varies	$\bar{\lambda}$ = 1	(d_{max}/d_{min}) = 1.66, d_{min} varies	$\bar{\lambda}$ = 1
E_c= 83 GPa	$\bar{E}_c$ = 83 GPa	E_c= 62 GPa	$\bar{E}_c$ = 62 GPa
(k_n/k_s) = 3.8 μ = 0.5	$\left(\overline{k^n}\ /\ \overline{k^s}\right)$ = 3.8 $\bar{\sigma}_c = \bar{\tau}_c$ = (mean $\pm$ std. dev.) =55.5 $\pm$ 35.5 MPa	(k_n/k_s) = 2.5 μ = 0.5	$\left(\overline{k^n}\ /\ \overline{k^s}\right)$ = 2.5 $\bar{\sigma}_c = \bar{\tau}_c$ = (mean $\pm$ std. dev.) =157 $\pm$ 36 MPa

2.2 Uniaxial Compression Simulation

Uniaxial compression simulations using PFC2D were performed to compare the physical properties of the created specimen model with those of the actual rock. The simulation was carried out using FISH scripting in PFC2D (Itasca Consulting Group, 2008). In the PFC2D uniaxial compression simulation, the specimen model was sandwiched between two frictionless walls, and loads were applied until the target compressive stress (10 MPa) of the input data was reached. Figure 2 shows schematics of the uniaxial compression simulations. The specimen models were 100 mm long and 50 mm wide.

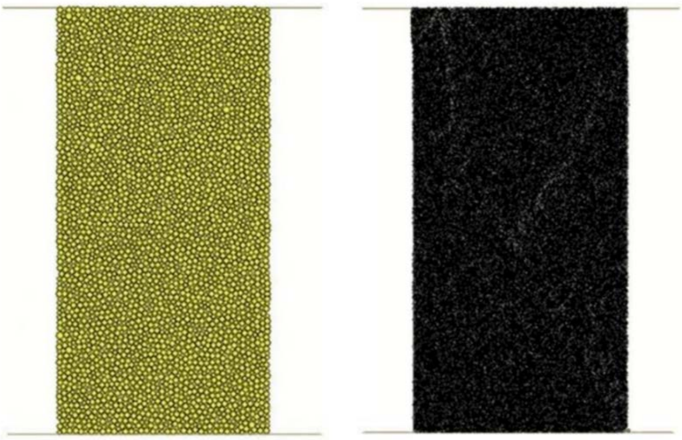

Figure 2: Schematics of the uniaxial compression simulations of the Carthage limestone (left) and Kurahashijima granite (right) specimen models. The specimens were compressed using the two frictionless walls indicated by the horizontal lines.

2.3 Rock Cutting Simulation

PFC2D was used to simulate drilling of the rock, and simulations were performed using typical geothermal well drilling conditions. The simulation was based on (Emam and Potyondy, 2010). The drilling conditions are shown in Table 2; input data for the PFC2D cutting environments are shown in Tables 3 and 4, and a schematic diagram of the cutting environment is shown in Figure 3. In the PFC modeling, a cutter (defined as a set of walls) moves horizontally over a synthetic rock mass at a specified speed and a constant depth of cut (see Figure 3). The synthetic rock sample, consisting of bound particles, is rectangular and confined by three frictionless walls on the bottom, left, and right sides. Mud column pressure in the lower hole is applied to the upper surface of the rock sample.

The cutter velocity in Tables 3 and 4, V (mm/s) is obtained from Equation 2.

$$V = 2\pi rN \tag{2}$$

Here,

r = Distance from bit center to bit cutter (mm)

N = Bit rotation speed (rev/s)

The Depth of cut, D_c (mm) is obtained from Equation 3.

$$D_c = R_p/N \tag{3}$$

R_p = Rate of drilling (m/hr)

Table 2: Drilling Conditions

Drilling depth, D (m)	1500
Density of mud water (water), ρ_w (kg/m^3)	1000
Bottomhole pressure (mud column pressure), P_{bh} (MPa)	15
Bit diameter, D_b (inches)	8-1/2
Bit rotation speed, N (rev/s)	2

Table 3: Input data for the PFC2D cutting environment for test A that considers the effect of the back-rake angle.

Simulation number	Carthage limestone	A-1	A-2	A-3
	Kurahashijima granite	A-i	A-ii	A-iii
Specimen height, H (mm)			100	
Specimen width, W (mm)			50	
Cutter length, l (mm)			40	
Cutter back-rake angle, θ (°)		20	15	10
Cutter velocity, V (mm/s)			1.4	
Confining pressure, P_{bh} (MPa)			15	
Depth of cut, D_c (mm)			0.7	
Use-gap flag; if set, then specify, G_f {G_a, G}			1	
Use absolute magnitude flag, G_a			0	
Gap value, G			1	
Rate of drilling (m/hr)			5	
Cutter position				

Table 4: Input data for the PFC2D cutting environment for test B that considers the effect of varying the cutter velocity and the depth of cut.

Simulation number	Carthage limestone	B-1	B-2	B-3	B-4
	Kurahashijima granite	B-i	B-ii	B-iii	B-iv
Specimen height, H (mm)		100			
Specimen width, W (mm)		50			
Cutter length, l (mm)		40			
Cutter back-rake angle, θ (°)		15			
Cutter velocity, V (mm/s)		1.4	0.45	1.4	0.45
Confining pressure, P_{bh} (MPa)		15			
Depth of cut, D_c (mm)		0.7	0.23	1.4	0.47
Use-gap flag; if set, then specify, G_f $\{G_a, G\}$		1			
Use absolute magnitude flag, G_a		0			
Gap value, G		1			
Rate of drilling (m/hr)		5		10	
Cutter position					

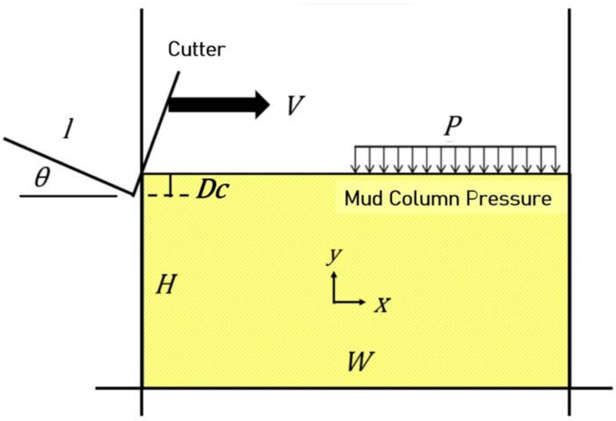

Figure 3: Schematic diagram of the cutting environment. The variables are defined in Table3. The yellow area is rock specimen.

Several simulations were performed using hard Carthage limestone and hard Kurahashijima granite as models, using different values for the digging rate, cutter position, cutter rake angle, cutter speed, and depth of cut. The simulations are divided into two main tests: (test A) a test in which suitable back-rake angles for each of the two specimen models were determined and compared with existing knowledge to confirm the validity of the single-cutter straight cutting simulation, and (test B) a test in which the most suitable back-rake angle for medium-hard rock determined in test A was used to simulate straight cutting of medium-hard rock and hard rock, while varying several conditions for the cutter and drilling rate. Also shown in Figure 4 is a schematic diagram of the simulated bit cutter arrangement. The bit circled in red is the outermost cutter and is located 108 mm from the bit center. The bit circled in blue is located 36 mm from the bit center.

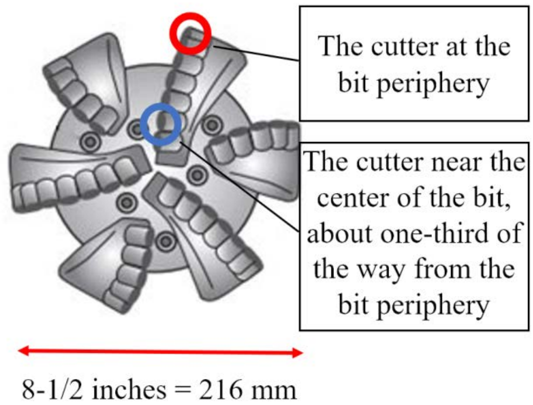

Figure 4: Schematic diagram of the simulated bit cutter arrangement.

3. Results and Discussion

3.1 Uniaxial Compression Simulation

Figure 5 shows the results of uniaxial compression simulations of limestone and granite. The red and blue lines in the specimen model represent tensile and shear failure, respectively. Table 5 compares Young's modulus and Poisson's ratio between the created specimen model and actual rocks. Uniaxial compressive strength is also shown. The Young's modulus and Poisson's ratio of the limestone and granite specimen models are within 5% of the Young's modulus and Poisson's ratio of the actual rocks. This confirms that the specimen models are correctly modeled as granular materials.

Table 5: Result of uniaxial compression simulation.

	Carthage Limestone			Kurahashijima Granite		
	Actual Rock	Specimen Model	Error (%)	Actual Rock	Specimen Model	Error (%)
Young's modulus (GPa)	76	79	3.8	72	72	0.0
Poisson's ratio	0.29	0.28	3.6	0.25	0.26	3.8
Uniaxial compressive strength (MPa)	NA	99	NA	NA	180	NA

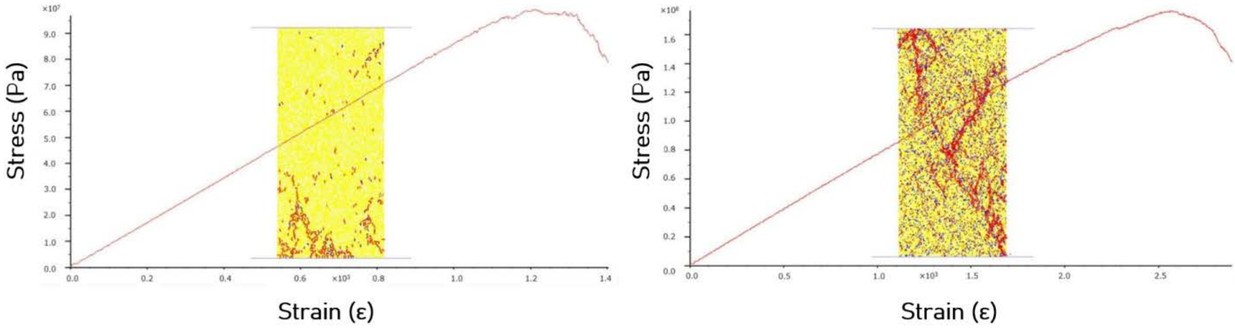

Figure 5: Stress-strain curves for Carthage limestone (left) and Kurahashijima granite (right). The image shows rock specimens where cracks created at 10 MPa are shown in red and blue lines.

3.2 Rock Cutting Simulation

<u>3.2.1 Back-Rake Angle (Simulations A-1 to A-3)</u>

This section presents the simulation results for different back-rake angles. The presented results include cutting schematics of the specimen, forces applied to the specimen, forces applied to the cutter, and specimen cracking. We also compare those results with existing experimental findings to confirm their validity. The specimen models were 50 mm long and 100 mm wide.

First, we consider results for the Carthage limestone specimen model. Figure 6 shows the cutting schematic diagram of the Carthage limestone specimen. The figure shows results for a 40-mm long horizontal cut, for which the influence of the leftmost boundary is minimal. The cutting schematic shows that a large back-rake angle results in more cracks near the cut surface, while a small back-rake angle results in more cracks inside the rock.

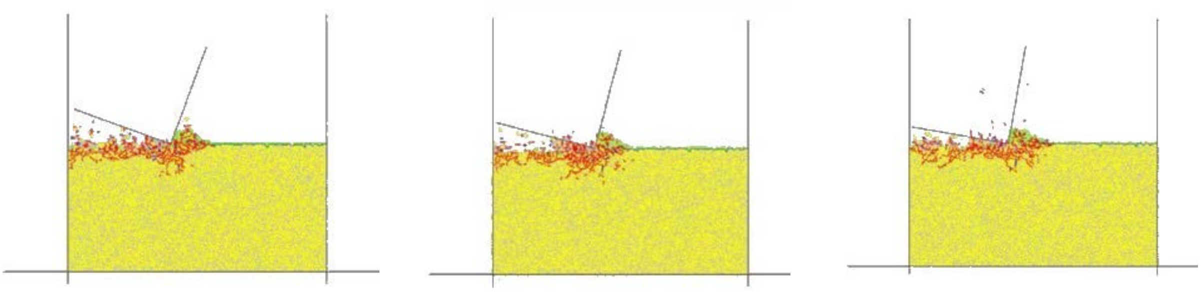

Back-rake angle; 20° **Back-rake angle; 15°** **Back-rake angle; 10°**

Figure 6: Simulated cutting behaviors of a single PDC cutter with different back-rake angles for Carthage limestone. The green lines represent the surface boundaries of the specimens; the red lines indicate cracks due to tensile failure, and the blue lines indicate cracks due to shear failure.

Figure 7 shows the results of the average stress applied to the specimen. The force applied to the specimen at horizontal penetration of 40 mm was greatest when the back-rake angle was 15°. The average stress on the specimen is always variable, with a maximum and a minimum. However, in the present simulation, the minimum value is about 0.04 mm, which is not reflected in the figure. Therefore, Table 6 shows the force that the sample receives from the cutter.

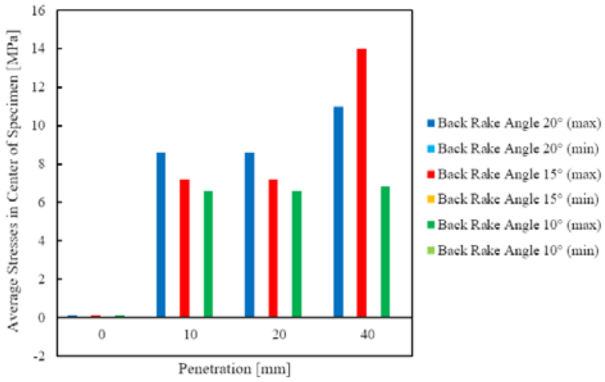

Figure 7: Effect of horizontal penetration on the average stress in the center of the Carthage limestone specimen for different back-rake angles.

Table 6: Simulation results of penetration depth on mean stress in the center of Carthage limestone specimen at different back rake angles.

Back-rake angle 20°		Back-rake angle 15°		Back-rake angle 10°	
Max Value	Min Value	Max Value	Min Value	Max Value	Min Value
0.12	-0.04	0.12	-0.04	0.12	-0.04
8.60	-0.04	7.20	-0.04	6.60	-0.05
8.60	-0.04	7.20	-0.04	6.60	-0.05
11.00	-0.04	14.00	-0.04	6.60	-0.05

Figure 8 shows the results of the forces applied to the cutter. The minimum and maximum forces on the cutter are shown separately for the x-axis and y-axis: the x-axis force is the horizontal force received by the cutter from the specimen as it moves horizontally to the right; the y-axis force is the vertical force received by the cutter as it pushes back in the positive y-axis direction to maintain a constant depth of cut. When the back-rake angle was 15°, the force applied to the cutter was greatest in the positive direction of the y-axis. This may be due to the amount of chips accumulated under the cutter pushing the cutter up in the positive direction of the y-axis to maintain a constant depth of cut. This suggests that the cutter bites into the rock surface was the case for the other back-rake angles tested.

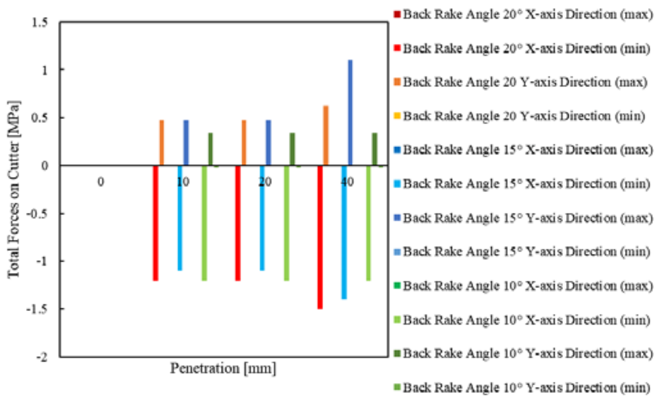

Figure 8: Maximum and minimum forces on the cutter at different horizontal penetrations in the Carthage limestone (x-axis and y-axis forces are shown separately).

Figure 9 shows a schematic diagram of the specimen at 40 mm cutting. The largest number of cracks appeared in the specimens when the back-rake angle was 15°. From these results, it can be inferred that a back-rake angle of 15° is suitable for medium-hard rock. Karasawa et al. (1991) conducted drilling tests using PDC core bits with back-rake angles ranging from 5° to 20°. According their findings, a back-rake angle of 5° to 20° is generally suitable for medium-hard rock. Furthermore, they found that using a back-rake angle of around 10° to 15° resulted in the best penetration rate. This is consistent with our simulation findings for the medium-hard Carthage limestone specimen.

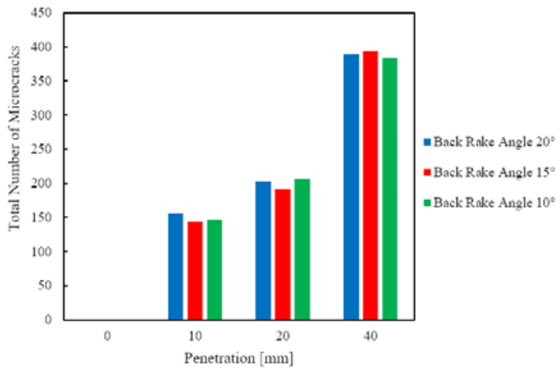

Figure 9: Total number of microcracks versus horizontal penetration of the Carthage limestone.

3.2.2 Back-Rake Angle (Simulations A-i to A-iii)

Next, we discuss the results for the Kurahashijima granite specimen model. Figure 10 shows a cutting schematic of a specimen of the Kurahashijima granite. As we did for the limestone specimen, we show results for a 40-mm long horizontal cut. The cutting schematic shows that a large back-rake angle results in more discrete cuttings near the cut surface, while a small back-rake angle results in fewer discrete cuttings and more prominent cracks in the rock interior. The specimen models were 50 mm long and 100 mm wide.

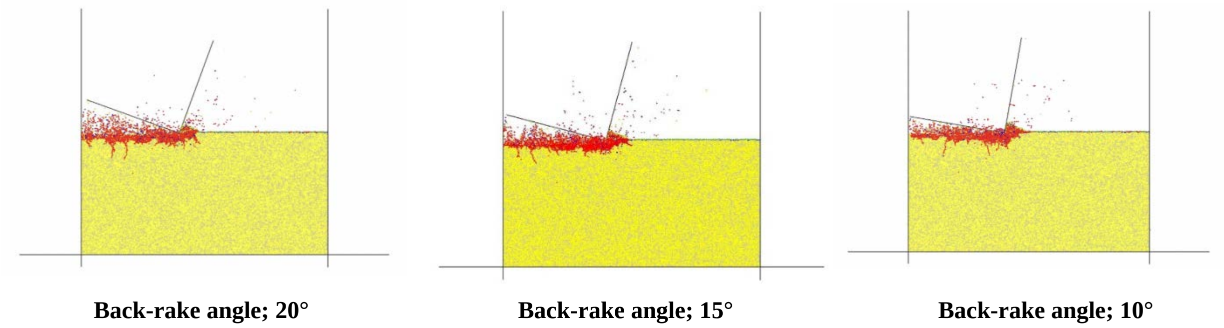

Figure 10: Simulated cutting behaviors of a single PDC cutter with different back-rake angles for Kurahashijima granite. The green lines represent the surface boundaries of the specimens; the red lines indicate cracks due to tensile failure, and the blue lines indicate cracks due to shear failure.

Figure 11 shows the results of the average stress applied to the specimen. There was no significant difference in the average stresses applied to the specimen when the back-rake angle was 20° and 15°.

Figure 12 shows the results of the forces applied to the cutter. When the back rake angle was 15°, the force applied to the cutter was greatest in the positive direction of the y-axis. Figure 13 shows the cracking results for the specimen. The specimen cracks were the largest when the back rake angle was 20°. From this result, it can be inferred that the specimen can be cut more efficiently at a back rake angle of 20° than at a back rake angle of 15° because the specimen is cracked with a smaller load on the cutter. From these results, it can be inferred that the 20° angle is suitable for hard rock. Similar to the results discussed above for limestone specimens, these results are consistent with the experimental results of Karasawa et al. (1991).

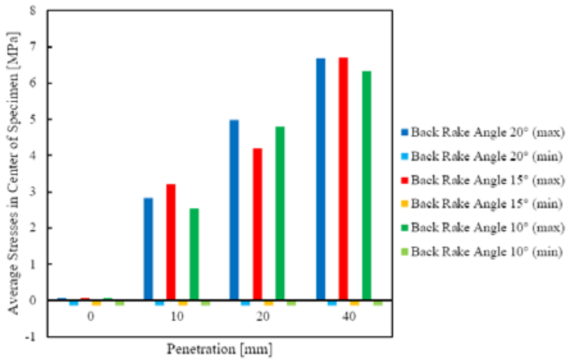

Figure 11: Effect of horizontal penetration on the average stress in the center of the Kurahashijima granite specimen for different back-rake angles.

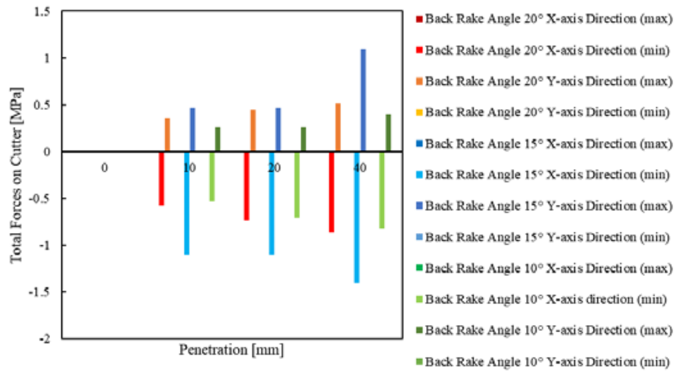

Figure 12: Maximum and minimum forces applied to the cutter for different horizontal penetrations of the Kurahashijima granite.

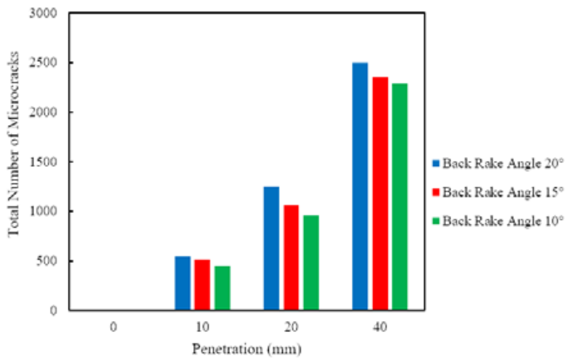

Figure 13: Total number of microcracks versus horizontal penetration of the Kurahashijima granite.

3.2.3 Cutting Simulations B-1 to B-4

For subsequent tests, we set the back-rake angle to 15° and simulated the cutting behavior of the two specimens for different drilling rates, cutter positions, cutter speeds and depths of cut. As in the previous sections, we consider the results of the cutting schematic, the forces applied to the specimen, the forces applied to the cutter, and the cracks in the specimen. The specimen models were 50 mm long and 100 mm wide.

First, we discuss the results for the Carthage limestone. Figure 14 shows schematic diagrams of the cutting.

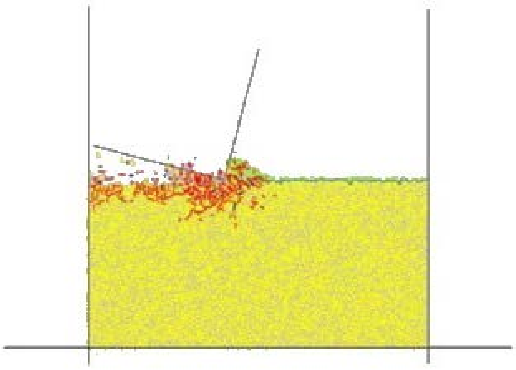

Simulation B-1

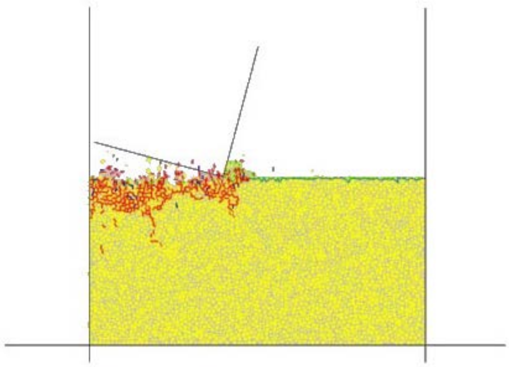

Simulation B-2

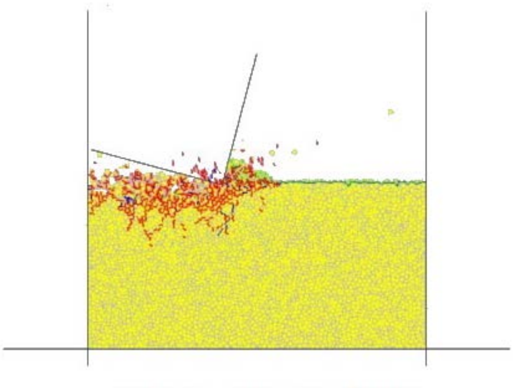

Simulation B-3

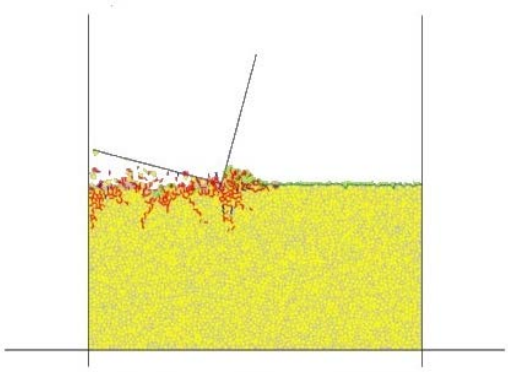

Simulation B-4

Figure 14: Simulated cutting behavior of the Carthage limestone specimen for different drilling configurations. The green lines in the figure represent the boundary surfaces of the specimens; the red lines indicate cracks due to tensile failure, and the blue lines indicate cracks due to shear failure.

Figure 15 shows the results of the average stress applied to the specimen. The average stress on the specimen is always variable, with a maximum and a minimum. However, in the present simulation, the minimum value is about 0.05 mm, which is not reflected in the figure. Therefore, Table 7 shows the force that the sample receives from the cutter. The stress applied to the specimen shows the highest value at a cutter speed of 1.4 mm/s and a cutter depth of 0.7 mm (B-1-max). The average stress on the specimen is always variable, with a maximum and a minimum. However, in the present simulation, the minimum value is about 0.05 mm, which is not reflected in the figure.

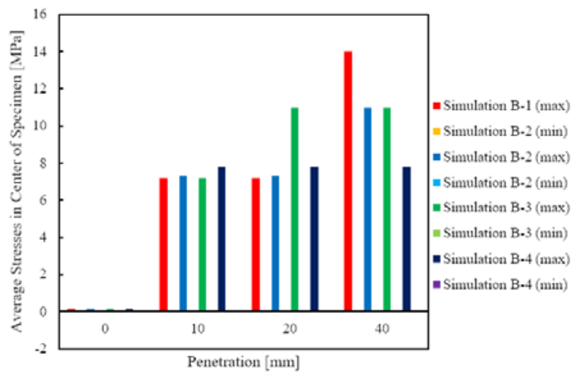

Figure 15: Effect of horizontal penetration on the average stress in the center of the Carthage limestone specimen for different drilling configurations.

Table 7: Simulation results of penetration depth on mean stress in the center of Carthage limestone specimen at different back rake angles.

Simulation B-1		Simulation B-2		Simulation B-3		Simulation B-4	
Max Value	Min Value	Max Value	Min Value	Max Value	Min Value	Max Value	Min Value
0.12	-0.04	0.12	-0.04	0.12	-0.04	0.12	-0.04
7.20	-0.04	7.30	-0.04	7.20	-0.05	7.80	-0.04
7.20	-0.04	7.30	-0.04	11.00	-0.05	7.80	-0.04
14.00	-0.04	11.00	-0.04	11.00	-0.05	7.80	-0.04

Figure 16 shows the results of the force applied to the cutter; the results in the x-axis direction show the smallest negative value when the cutter speed is 1.4 mm/s and the depth of cut is 1.4 mm (B-4 X-axis Direction-min). This result suggests that cuttings accumulate in front of the cutter at the outermost position of the bit when the bit rotation speed is high; the result in the y-axis direction shows the largest value when the cutter speed is 0.45 mm/s and the depth of cut is 0.47 mm (B-4 Y-axis Direction-max). From these results, it can be inferred that cuttings accumulate under the cutter located close to the bit center when the bit rotation speed is slow. Figure 17 shows the cracking results for the specimen. The specimen cracks are the largest when the cutter speed is 1.4 mm/s and the depth of cut is 1.4 mm (B-3).

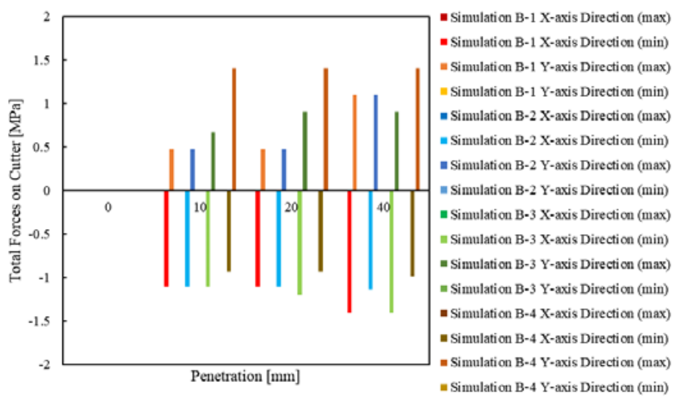

Figure 16: Maximum and minimum forces applied to the cutter for different horizontal penetrations of the Carthage limestone and different drilling configurations.

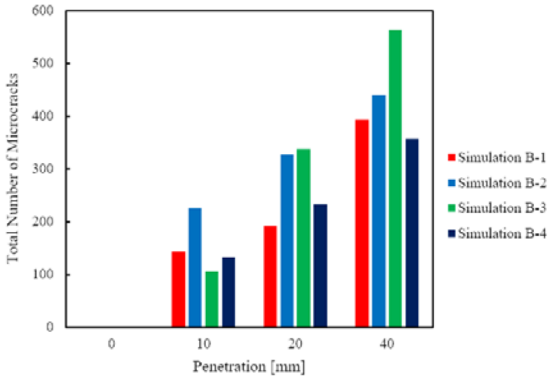

Figure 17: Total number of microcracks versus horizontal penetration of the Carthage limestone.

3.2.4 Cutting Simulations B-i to B-iv

Next, we discuss the results of the simulations for the Kurahashijima granite. As in the previous section, we discuss the results for the cutting schematic, forces applied to the specimen, forces applied to the cutter, and cracks in the specimen. Figure 18 shows the cutting schematic results. The specimen models were 50 mm long and 100 mm wide.

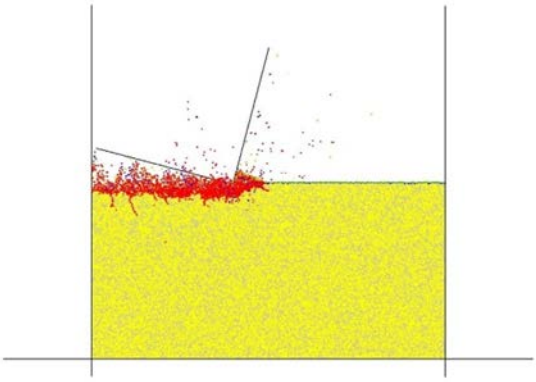

Simulation B-i

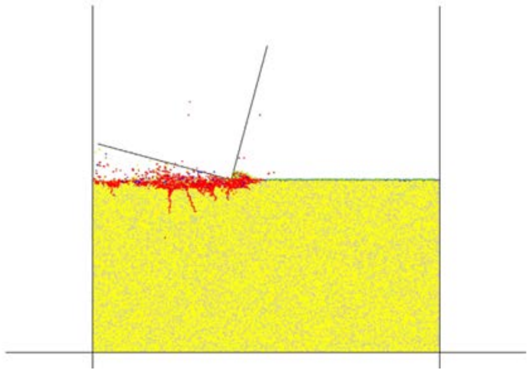

Simulation B-ii

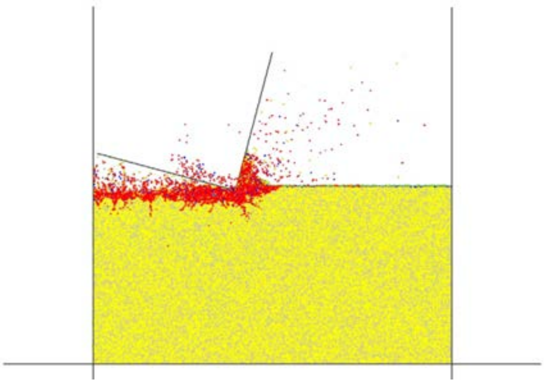

Simulation B-iii

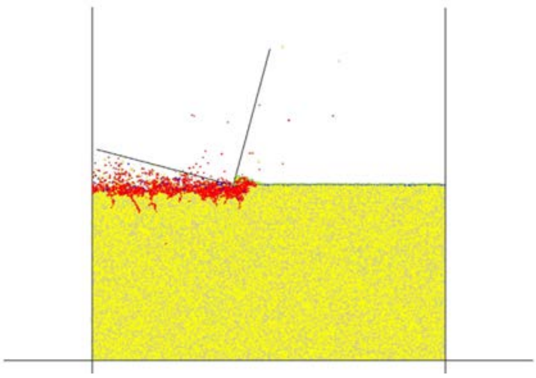

Simulation B-iv

Figure 18: Simulated cutting behavior of the Kurahashijima granite specimen for different drilling configurations.

Figure 19 shows the results of the stress applied to the specimen. The stress applied to the specimen shows the highest value at a cutter speed of 1.4 mm/s and a depth of cut of 1.4 mm (B-iii-max).

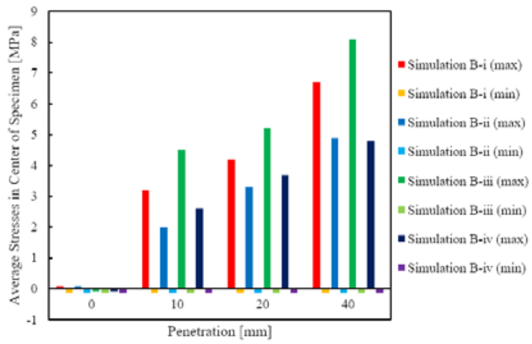

Figure 19: Effect of horizontal penetration on the average stress in the center of the Kurahashijima granite specimen for different drilling configurations.

Figure 20 shows the results of the force applied to the cutter; the x-axis direction results show the largest negative value when the cutter speed is 1.4 mm/s and the depth of cut is 0.7 mm (B-i X-axis Direction-min). From this result, it can be inferred that cuttings accumulate the most in front of the cutter at the outermost position of the bit when the bit rotation speed is high; the result in the y-axis direction shows the largest value when the cutter speed is 1.4 mm/s and the depth of cut is 0.7 mm (B-i X-axis Direction-max). From these results, it can be inferred that the cuttings accumulate the most under the cutter at the outermost position of the bit when the bit rotation speed is high.

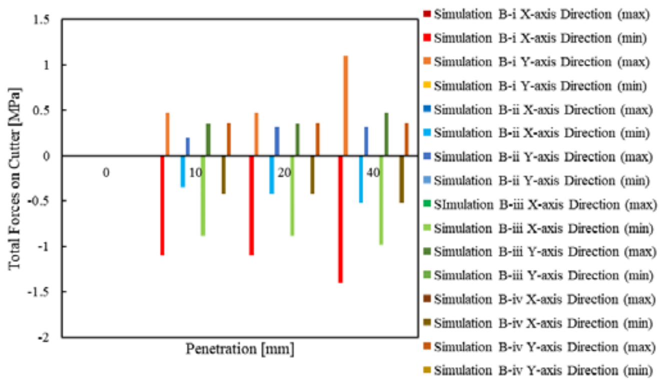

Figure 20: and minimum forces applied to the cutter for different horizontal penetration of the Kurahashijima granite and different drilling configurations.

Figure 21 shows the cracking results for the specimen. The maximum cracking of the specimen occurs when the cutter speed is 1.4 mm/s and the depth of cut is 1.4 mm (B-iii).

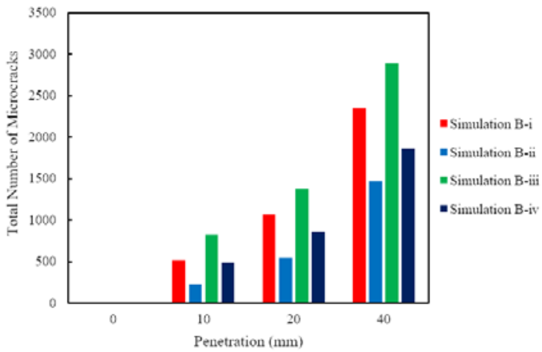

Figure 21: Total number of microcracks versus horizontal penetration of the Kurahashijima granite.

5. Conclusion

Numerical simulation results for optimizing the design and operating conditions of a PDC bit for drilling and scraping medium-hard to hard formations revealed the following.

1. Discrete element method simulations revealed the cracks and number of cracks inside the rock, the stresses applied to the rock, and the forces applied to the cutter. From the simulation results, it was inferred that when excavating medium-hard to hard formations with a PDC bit, a relatively high bit rotation speed would allow for more efficient drilling.

2. The results of the mean stresses applied to the specimens by the cutter indicate that the mean stresses on the specimens are lower for medium-hard rock and higher for hard rock when the back-rake angle is 15° and the rate of drilling is increased.

3. The results of the force applied to the cutter allowed for a rough comparison of the volume of broken cuttings.

REFERENCES

Emam, S., and Potyondy, D. "PFC2D Rock-Cutting Procedures." Technical Memorandum ICG7156-L, Itasca Consulting Group, Inc., (2010).

Potyondy, D. O., and Cundall, P.A. "A Bonded-Particle Model for Rock." *International Journal of Rock Mechanics & Mining Sciences,* 41(8), 1329–1364, (2004). https://doi.org/10.1016/j.ijrmms.2004.09.011

Itasca Consulting Group, Inc. "FISH in PFC2D." (2008).

Kaneko, M., Murata, K., Shiba, T, and Omi, M. "Elastic Modulus of Granite and Its Evaluation -Fundamental Study on Evaluation Method of Deformability of Rock Mass (Report 2)." *Journal of the Japan Mining Industry Association*, 103(1187), 9–15, (1987). (In Japanese) https://doi.org/10.2473/shigentosozai1953.103.1187_9

Karasawa, H., Misawa, S., and Yoshida, S. "Studies on Optimum Rake Angles for PDC Bits." *Journal of the Japan Society of Natural Resources and Materials*, 107(12), 853–858, (1991). (In Japanese) https://doi.org/10.2473/shigentosozai.107.853